Int J Adv Manuf Technol (2017) 93:4043–4061
DOI 10.1007/s00170-017-0880-2

ORIGINAL ARTICLE

An approach to evaluate delamination factor when drilling carbon fiber-reinforced plastics using different drill geometries: experiment and finite element study

Sinan Al-wandi[1] · Songlin Ding[1] · John Mo[1]

Received: 5 May 2017 / Accepted: 24 July 2017 / Published online: 1 August 2017

Abstract Delamination is one of the major damages associated with drilling carbon fiber-reinforced plastics (CFRP), Peel-up and Push-out are two recognizable delamination mechanisms, while drilling without using a back-up plate under the workpiece complicates the delamination mechanism even more. Minimizing delamination is dependent on many factors such as cutting parameters, geometry and type of drill bits used. The objective of this study is to present a new approach to measure the equivalent adjusted delamination factor (F_{eda}) when drilling unidirectional CFRP laminates without using a back-up plate and comparing it experimentally and numerically with conventional delamination factor (F_d) and adjusted delamination factor (F_{da}). A polycrystalline diamond (PCD) twist drill and a special diamond coated double point angle drill was used for drilling in this study. The 3D finite element model was developed in ANSYS-Explicit to simulate the drilling process using the ply-based modeling method instead of a conventional zone-based concept. Experimental drilling validation process was implemented by utilizing a CNC machining center. Results show that the F_{eda} obtained is suitable to estimate the drilling induced damages, damage analysis shows that good agreements were obtained from the experiments and finite element method (FEM) simulation, while the special diamond coated double point angle drill seemed to provide a better hole quality, and drilling induced damage is highly affected by feed rate which is considered one of the important parameter.

✉ Sinan Al-wandi
s3362028@student.rmit.edu.au

[1] School of Engineering, RMIT University, Melbourne, Australia

Keywords Drilling · Delamination · FEM · PCD · CFRP

1 Introduction

Each year there is a growing demand for composite materials such as CFRP to fulfill requirements in the field of mobility, transport, aerospace, marine, civil, chemical, and sport equipments to reduce fuel consumption and CO_2 emissions [1, 2], and combines high strength, high stiffness, and low weight [3]. Drilling holes is of high importance to the aviation industry [4], and a high rate of components do not pass quality inspection due to the undesired delamination, and can be omitted when using the appropriate cutting tools and parameters [5]. The present approach of utilizing non-destructive assessment such as eddy current, radiography, thermography, C-scan, and so forth is costly, tedious, and often cannot be implemented on structures placed in service due to the unavailability of hardware required to perform the test [6], currently numerical modeling is utilized as a tool for a superior comprehension of machining of these composites.

In the literature, Durão et al. [7] studied the delamination assessment techniques based totally on radiographic information compared with mechanical test outcomes. Results show an adequate feed rate and tool geometry combination should be used to eliminate delamination effects when drilling holes. Grilo et al. [8] carried out an experimental assessment and found that both delamination factor and adjusted delamination factor were appropriate for delamination assessment in drilling CFRP.

Tsao et al. [9] described a novel method for reducing delamination through the use of active backup force during drilling of composites. The backup force majorly suppressed the growth of delamination at drilling exit by

60−80%. Shyha et al. [10] outlined the analysis of hole quality/integrity when drilling titanium/CFRP/aluminium stacks with uncoated and coated CVD diamond and hard metal tungsten carbide drills. Results showed delamination of CFRP laminates were considerably decreased due to the Al and Ti supported layers.

To determine the optimal process parameter levels and to analyze the effect of parameters on delamination factor, Gaitonde et al. [11] introduced the methodology of Taguchi optimization approach for reducing the delamination at the hole entrance of CFRP composites when using high speed drilling, results show the most significant factor is point angle then feed and spindle speed.

Tsao [12] experimentally studied the prediction of thrust force of step drill with different drilling parameters in drilling CFRP laminates; the study was based on Taguchi method and radial basis function network, and results show the overall performance is dramatically affected by step angle, feed rate and stage ratio.

The finite element analysis (FEA) method is an alternative approach for tedious and costly experimental analysis, and provides an insight of the cutting process, and is very much required for a reliable prediction and optimal stress and damage results [13].

Progresses in computational power prompted the improvement of numerical techniques and modeling tools [14]. Niezgoda and Derewońko [15] proposed a global-local (meso) modeling technique to minimize the computational effort in assessing composite structures. The amount of nodes and elements utilized in the meso-scale approach is around 60% less than in the micro-scale approach, this will allow assessing a 3D composite structure with different fiber orientations in a sensible amount of time.

To analyze the hypervelocity impact damage in composite laminates, Cherniaev and Telichev [16] developed a numerical meso-scale approach of a laminate composite totally based on detailed representation of meso-scale technique, the material models in regards to laminate structure are appropriate for explicit modeling. Stier et al. [17] modeled a meso-scale representative volume element (RVE) of a twill weave CFRP ply comprised of the yarn part, and the surrounding matrix region. The results for experiment and numerical tests for large shear strains at large deformations were different from each other, however, at small deformations were in good agreement.

By using finite element analysis, Han and Chang [18] analyzed the failure modes to determine the material failure subjected to loading for a type III hydrogen pressure vessel, utilizing the ply-based approach to model the composite laminates. Results showed accurate stress distribution in the layers of the composite provided by the ply-based modeling approach, and despite of layers showed delamination or matrix failure, the general structure was reliable.

However, there is still lack of research in implementing ply-based modeling and validating its results, and due to the very challenging task in modeling composites using conventional zone-based methods, a ply-based modeling allows firstly the manufacturability of the composite product can be assessed, areas where the reinforcement cannot follow the surface are indicated and hence measures can be taken in design to avoid this. Secondly, the simulation gives the actual fiber orientations at any location in the model. This information is critical for accurate finite element analysis of the structure.

In this paper, a new delamination factor was proposed to investigate the operating parameters on the drilling induced damage hole entrance peripheral using a PCD twist drill and a special diamond coated double point angle drill when drilling unidirectional CFRP laminates. A new 3D finite element model for predicting the thrust force, torque, and delamination at planned feed rate and speed combinations was implemented using the ply-based modeling technology to model the laminates using the classical laminate theory keeping the laminates bonded together. Experimental cutting tests were conducted and results were compared with the finite element analysis results to validate the proposed model. Scanning electron microscopy (SEM) and microscopy image processing instruments and ImageJ software were used in obtaining the delaminated areas.

2 Experiment setup and materials

The workpiece used in the drilling experiment was unidirectional CFRP VTM264 which is 4 mm in thickness; it was prepared using the hand lay-up process.

Two different types of 8 mm two-flute diamond drill bits (PCD twist drill and diamond coated double point angle drill) made by “SECO” were utilized in the experiment, while Table 1 shows the geometric parameters of the drill bits. To validate the new model, cutting experiments were conducted and drilling tests were carried out on 3-axis HAAS CNC machining center. A six-channel dynamometer (Kistler 9257B) was used to measure the thrust force and torque. An eight-channel coupler (Kistler 5070A) was used to amplify the signals which were transferred to the data acquisition card (NI DAQ DE6213). Figure 1 shows the schematic drawing and experimental setup of the system.

3 Finite element analysis

3.1 Ply-based modeling

Ply-based model and zone-based model are the two basic methodologies commonly employed to create composite

Table 1 Geometric parameters of the drill bits

Drill type	Drill diameter	Point angle	Helix angle	Number of flutes
PCD twist drill	8 mm	120°	30°	2
Diamond-coated Double point angle drill	8 mm	60°–130°	30°	2

models. Ply-based models are developed based on each ply in a composite; material properties and local orientations are assigned to each ply, while zone-based models discretize the composite into zones of effective properties, each zone is aligned a material property based on the ply-stacking and fabric deformation.

To describe an arbitrary composite layup, a ply-based concept is much more realistic than a zone-based concept because ply-based means manufacturing-based. In the ply-based concept, it is simple to add or delete plies at any location. Figure 2 shows a simple plate made by four plies. Each ply has different size and orientation, particularly layer 4 is diagonally oriented. In a zone-based approach, the plate has to be divided into eight zones with different thickness and different fiber direction across the thickness [19]; however, a ply-based approach only requires four plies to capture the behavior of the entire structure, this will significantly make modifying the model easier if it is required.

Modeling of the cutting tool is very important to finite element (FE) simulation. The model must represent the dynamic change of the tool's physical properties during machining. A simplified rigid body cutting tool, which is currently used by the vast majority of researchers when drilling CFRP in their FE simulation, is not able to predict correctly the effect of process parameters on drilling CFRP.

Fig. 1 Experimental setup

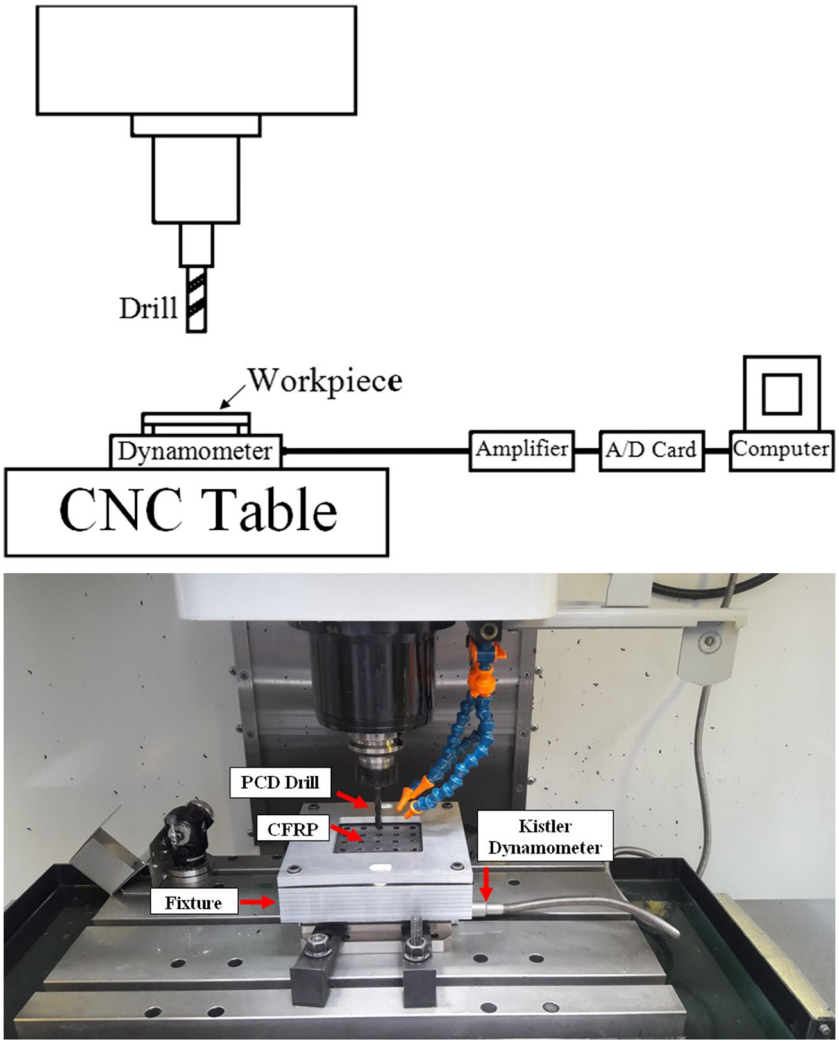

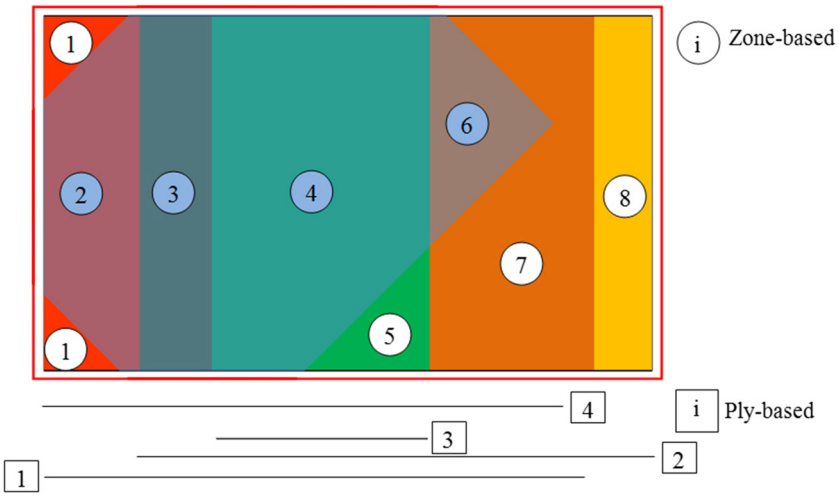

Fig. 2 Zone-based vs. ply-based

In this study, we intend to capture and predict the dynamic effect of machining parameters on the CFRP workpiece as well as the inflected stresses on the cutting tool, hence the drill was modeled as a flexible body.

Machining temperature is an important factor when machining CFRP. and if the machining temperature is higher than the glass transition temperature (Tg) of the resin will degrade the strength and properties of the CFRP [20]. Ha et al. [21] concluded that during high-speed machining of CFRP under dry conditions, the cutting temperature increases when increasing the cutting speed, leading to melting epoxy resin and resulting in the chips changing from powder to spalling. And to prevent any unexpected high temperatures and also carbon dust during the drilling process, a high amount of coolant was used in the experiments and heat generation in the simulation process was not considered.

3D Lagrangian formulation FE models of CFRP composite and twist drill and double point angle drill (Fig. 3) were developed using ANSYS-EXPLICIT and AUTODYN software, both drills were meshed with solid185 eight node linear tetrahedral elements. A uni-directional CFRP composite laminate with stack sequence of [(0/90)2]s which was used in the FE analysis has dimensions of

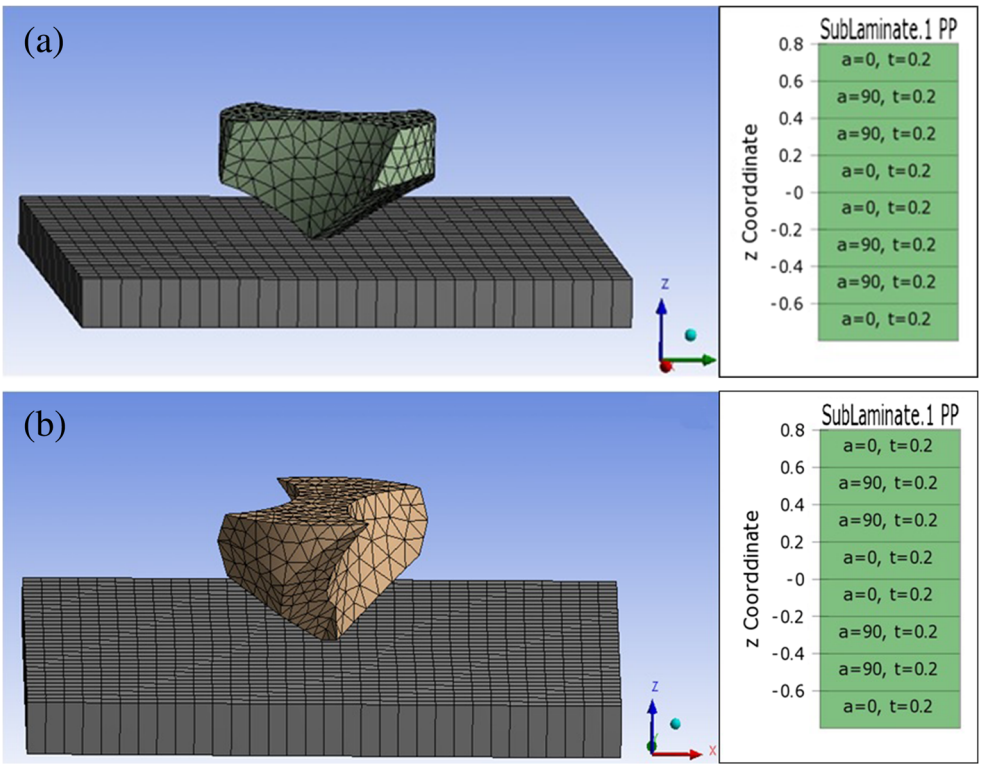

Fig. 3 Finite element model of VTM264 CFRP laminate with **a** PCD twist drill and **b** diamond-coated double angle drill

Table 2 Cutting parameters used in drilling

Drilling parameter	Magnitude
Drill diameter (mm)	8
Spindle speed (rpm)	2500, 5000, 7500, 10000
Feed (mm/rev)	0.05, 0.10, 0.125
Feed rate (mm/min)	125, 500, 1250

20 mm × 20 mm × 1.6 mm and consists of eight plies. The thickness of each ply was 0.2 mm. The workpiece was meshed with shell181 four node linear quadrilateral elements.

The boundary conditions were enforced on the drills and workpiece to enable simulation process. Both drills were located at the top center of the workpiece and was made to rotate (angular velocity) around the Z axis (urz) and moved in the cutting direction (uz). The workpiece was fixed from the sides from moving (ux = uy = uz = 0). The cutting parameters applied in the experiments are listed in Table 2.

Meso-scale modeling is an approach of modeling properties and mechanisms of deformation and failure of functional and structural materials at various scale levels, with different loads [22], it is the intermediate level between micro-mechanics and macro-mechanics.

The modeling approach comprises the involvement of the main micro-mechanisms controlling the materials mechanical behavior and failure and the applicability of the continuum mechanics equations. Therefore, it is used in this study to close the gap between the complex failure mechanisms of the micro-mechanics analysis and the empirical and case specific of the macro-mechanics analysis.

The material model used for the workpiece was orthotropic homogeneous elastic assigned according to the fiber orientation through a defined local coordinate system. Table 3 shows properties of the orthotropic unidirectional material VTM264 [23]. Table 4 shows the strength properties of the unidirectional laminate while Table 5 shows the general properties of diamond used in the drilling tool.

3.2 Constitutive material model of unidirectional CFRP

Progressive damage modeling of polymer matrix composites as a predictive capability for the complex nonlinear behavior of these materials has been used. Intralaminar and interlaminar damage mechanisms are the basis of fracture process of composites which include fiber breakage, matrix cracking, and delamination.

Table 4 Strength properties of unidirectional VTM264 laminate

Property	Magnitude (MPa)
0° Tensile strength	2575
90° Tensile strength	40
0° Compressive strength	1235
90° Compressive strength	182
In-plane shear strength (IPSS)	85.7
0° Interlaminar shear strength (ILSS)	88.6

The most common fracture mode is interlaminar delamination; it is prompted by shear and normal stresses at the interface of adjoining layers in CFRP laminate [24].

Due to experimental difficulties caused by the typical extensive fiber bridging, which makes the insertion of initial defect difficult for the fracture toughness test. The following constitutive material in the FE model was used to find out how intralaminar delamination effects the first ply failure.

The orthotropic material model for shell layers developed can be expressed as in-plane stress-strain relationship [25]:

$$\sigma_i = c_{ij}\epsilon_j \tag{1}$$

By setting:

$$\sigma_3 = 0 \;\; \tau_{23} = 0 \;\; \tau_{31} = 0 \tag{2}$$

The stress-strain relation in terms of reduced stiffness is:

$$\begin{bmatrix} \sigma_1 \\ \sigma_2 \\ \tau_{12} \end{bmatrix} = \begin{bmatrix} Q_{11} & Q_{12} & 0 \\ Q_{12} & Q_{22} & 0 \\ 0 & 0 & Q_{66} \end{bmatrix} \begin{bmatrix} \epsilon_1 \\ \epsilon_2 \\ \gamma_{12} \end{bmatrix} \tag{3}$$

Whereas in terms of engineering terms:

$$\begin{aligned} Q_{11} &= \frac{E_1}{1-\nu_{12}\nu_{21}}, Q_{22} = \frac{E_2}{1-\nu_{12}\nu_{21}} \\ Q_{66} &= G_{12}, Q_{12} = \frac{\nu_{12}E_2}{1-\nu_{12}\nu_{21}} = \frac{\nu_{21}E_1}{1-\nu_{12}\nu_{21}} \end{aligned} \tag{4}$$

The stress-strain relationship becomes:

$$\begin{bmatrix} \sigma_{11} \\ \sigma_{22} \\ \tau_{12} \end{bmatrix} = \begin{bmatrix} \frac{E_1}{1-\nu_{12}\nu_{21}} & \frac{\nu_{21}E_1}{1-\nu_{12}\nu_{21}} & 0 \\ \frac{\nu_{12}E_2}{1-\nu_{12}\nu_{21}} & \frac{E_2}{1-\nu_{12}\nu_{21}} & 0 \\ 0 & 0 & G_{12} \end{bmatrix} \begin{bmatrix} \epsilon_{11} \\ \epsilon_{22} \\ \gamma_{12} \end{bmatrix} \tag{5}$$

Whereas σ is the normal stress, C is stiffness tensor, ϵ is the normal strain, τ is the shear stress, E is the modulus of elasticity, γ is the shear strain, G is the shear modulus, ν is the Poisson's ratio, and Q is the reduced stiffness.

Table 3 Mechanical properties of unidirectional VTM264 laminate

E11	E22	E33	v12	v13	v23	G12	G13	G23	Ply thickness
117 GPa	7.47 GPa	7.47 GPa	0.33	0.02	0.33	4.07 GPa	4.07 GPa	2.31 GPa	0.2 mm

Table 5 General properties of diamond used in the drilling tool

Property	Magnitude	Units
Hardness	10,000	kg/mm^2
Strength, tensile	> 1.2	GPa
Strength, compressive	> 110	GPa
Fracture strength	400–800	MPa at < 1 mm thickness
Density	3.52	g/cm^3
Young's modulus	1200	GPa
Poisson's ratio	0.2	Dimensionless
Thermal expansion coefficient	1.1–5.0 (300–1300 K)	ppm/K
Thermal Conductivity	10–20	W/cm-K
Coefficient of friction	0.05 (dry)	Dimensionless

3.3 Intralaminar, interlaminar, and shear stresses

To reduce the computational time, and in the meantime, ensure the high accuracy of predictive outcomes, shell elements of layered composite structures is applied based on the first-order shear deformation theory (FSDT) in analyzing intralaminar, inerlaminar, shear stresses, and transverse shear stresses.

Figure 4 shows a cylindrical coordinate system for describing an arbitrary doubly curved shell [26].

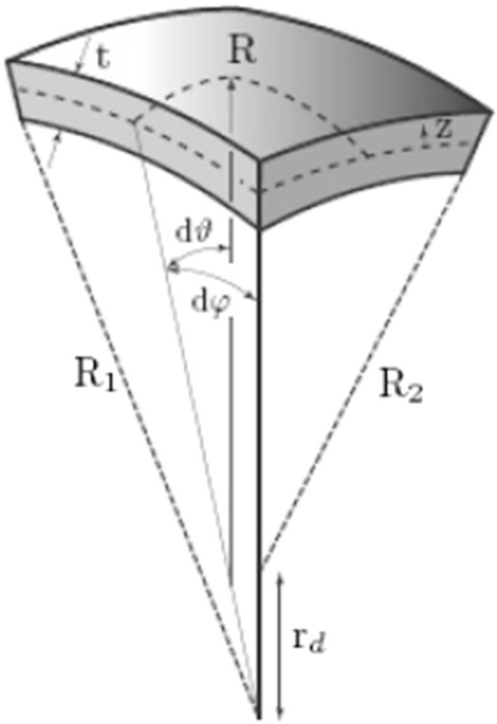

Fig. 4 Doubly curved FE geometry

The differential equation of the through-the-thickness displacement is [27]:

$$0 = w_{,rr} + w_{,r}\left(\frac{1}{r} + \frac{1}{r + r_d}\right) + w\left(\frac{\widehat{C}_{13} + \widehat{C}_{23} - 2\widehat{C}_{12}}{r(r + r_d)} - \frac{\widehat{C}_{11}}{r^2} - \frac{\widehat{C}_{22}}{(r + r_d)^2}\right) + P \quad (6)$$

$\widehat{C}_{ij} = \frac{\overline{C}_{ij}}{\overline{C}_{33}}$ and P is

$$P = u_{,\varphi}\left(\frac{\widehat{C}_{13} - \widehat{C}_{12}}{r(r + r_d)} - \frac{\widehat{C}_{11}}{r^2}\right) + u_{,\varphi r}\frac{\widehat{C}_{13}}{r} + v_{,\vartheta}\left(\frac{\widehat{C}_{23} - \widehat{C}_{12}}{r(r + r_d)} - \frac{\widehat{C}_{22}}{(r + r_d)^2}\right) + v_{,\vartheta r}\frac{\widehat{C}_{23}}{r + r_d} + \epsilon_i^F\left(\frac{\widehat{C}_{1i} - \widehat{C}_{3i}}{r} + \frac{\widehat{C}_{2i} - \widehat{C}_{3i}}{r + r_d}\right) \quad (7)$$

Whereas $\overline{C}_{ij}$ are the components of the three-dimensional stiffness matrix expressed in reference coordinates. P is the particular part of the differential equation.

$r = R_1 + z,\ r_d = R_2 - R_1$ and $z = [-t/2, t/2]$

u,v,w are displacements in the cylindrical coordinate system; r is radial ordinate; r_d is radius difference; z is thickness coordinate; t is the thickness; R_1 and R_2 are the constant curvature radii of the centerline; d_φ and d_ϑ are the apex angles for angular segments.

3.4 Constitutive damage initiation and evolution

Failure occurs when either of the stress components reaches the yield stress, and in this case, we can observe the occurrences of damage and progressive failure. While damage can advance in several directions in the model near and

around the weakest elements, "Matrix Cracking" is usually the first damage to happen as the matrix has the lowest stress for failure [28].

When panels and plates during service are subjected to in-plane multi axial stress, then failure is prompted and significantly affected by the in-plane shear stress depending on the sequence of the stacking. To estimate the damage initiation and evolution, we must first identify the type of group it falls into, as there are two groups of failure criteria exist.

(i) Independent failure criteria: The interactions between several stress components are neglected.
(ii) Polynomial failure criteria: The interactions between several stress components are considered.

Independent failure criteria include the maximum stress criteria and the maximum strain criteria. The stress and strain components in these criteria do not have any dependence between them; this means that the components in the longitudinal, transverse, and stacking directions do not affect each other.

Polynomial failure criteria include polynomial maximum stress criterion, Tsai-Wu, Tsai, Tsai-Azzi, Tsai-Hill, polynomial maximum strain criterion, Hoffman criteria, and Hashin criteria, the components in each direction depends on each other.

Hashin damage mechanism and failure criterion are used here to simulate the damage process of matrix and fiber. The failure criterion is formulated under tensile and compressive loads in longitudinal and transverse direction of fiber respectively and the interaction between the four failure modes shown in Eqs. 8 to 11 [29] are taken into account and therefore Hashin failure was used in the finite element analysis.

One of the requirements for this criteria is to have the lamina properties, and it can be experimentally determined easily. Moreover, it can give numerically solid results when the criteria is applied for first ply failure load in glass and carbon fibre composites.

Tensile fiber mode

$$(\frac{\sigma_{11}}{\sigma^f_{11t}})^2 + (\frac{\sigma_{12}}{\tau^f_{12}})^2 = 1 \qquad \sigma_{11} > 0 \tag{8}$$

Compressive fiber mode

$$(\frac{\sigma_{11}}{\sigma^f_{11c}})^2 = 1 \qquad \sigma_{11} \leq 0 \tag{9}$$

Tensile matrix mode

$$(\frac{\sigma_{22}}{\sigma^f_{22t}})^2 + (\frac{\sigma_{12}}{\tau^f_{12}})^2 = 1 \qquad \sigma_{22} > 0 \tag{10}$$

Compressive matrix mode

$$(\frac{\sigma_{22}}{2\tau^f_{12}})^2 + [(\frac{\sigma^f_{22c}}{2\tau^f_{12}})^2 - 1](\frac{\sigma_{22}}{\sigma^f_{22c}}) + (\frac{\tau_{12}}{\tau^f_{12}})^2 = 1 \quad \sigma_{22} \leq 0 \tag{11}$$

Whereas f denotes fiber, t is tension, and c is compression.

When any Hashin's criteria have been fulfilled in any mode in the equations above, damage will be initiated.

Without damage initiation criteria, the damage evolution law has no effect on the material. The damage evolution law defines the way a material degrades following the initiation of damage and progressive damage generally refers to degradation of stiffness, the stiffness reduction takes a value of 0 to 1, where 0 is no damage and 1 is completely damaged.

The evolution law of the damage variable in the post-damage initiation phase can also be based on the fracture energy dissipated (Gc) during the damage process. The damage variable can be defined from the equation below [30]:

$$D = \frac{\delta^f_m(\delta^{max}_m - \delta^0_m)}{\delta^{max}_m(\delta^f_m - \delta^0_m)} \tag{12}$$

Whereas δ^f_m is the mixed-mode displacement at complete failure, δ^{max}_m refers to the maximum value of the mixed-mode displacement, and δ^0_m is the effective displacement at the damage initiation.

Gc can be found from the area under the triangle shown in Fig. 5, and the failure displacement can be calculated as follows:

$$\delta^f_m = \frac{2Gc}{\sigma^0_m} \tag{13}$$

whereas δ^0_{eq} and δ^f_{eq} are the equivalent displacements.

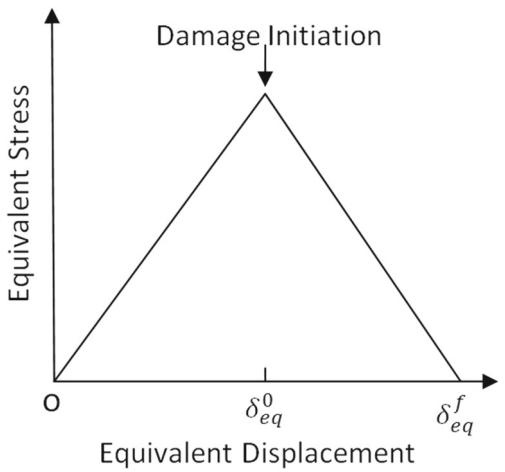

Fig. 5 Damage initiation and evolution

4 Damage evaluation methodology

Peel-up delamination and push-down delamination are the two main types of damage that are different in causes and effects while drilling CFRP. Damage extension can be evaluated through non-destructive test (NDT) such as acoustic emission, enhanced radiography, C-scan, and computerized tomography (CT) [14].

In the majority of these methods, the objective is to acquire images that outline the surrounding areas of the hole to further measure and analyze diameters and areas. In this study, a PhilipsXL30 SEM was used to obtain the delaminated vicinity areas of entrance of the holes drilled by the PCD twist drill. For the SEM in particular, the specimens were first surface-coated with a thin layer of gold before observation; a Leica optical microscope was used in obtaining the images of the delaminated vicinity of entrance of the holes drilled by the diamond-coated double-point angle drill; both instruments were successful in obtaining the required delaminated areas while the software "ImageJ" was utilized to process the image of delaminated areas. The delaminated areas appear in white, while the undamaged areas are in black as shown in Fig. 11a, then a selected parameters from the software for the binary image is chosen such as image enhancement, noise filtering, brightness, and edge detection to obtain an acceptable quality for the damaged areas which are then selected and copied into a white background and switching the color of the damaged area from white to black as shown in Fig. 11b.

Delamination factor F_d, the ratio of the maximum diameter (D_{max}) of the delamination zone to the nominal hole diameter (D_{nom}) as in Eq. 14, is widely used to characterize the level of delamination damage on composite materials. But the delamination criterion based on delamination factor cannot be satisfactory because the delamination caused by few peeled up or pushed down does not predict the real delamination zone of the drilled hole periphery. Therefore, a more accurate two dimensional delamination factor is needed as in Eq. 15; Fig. 6 shows the scheme of delamination in drilling composite laminate.

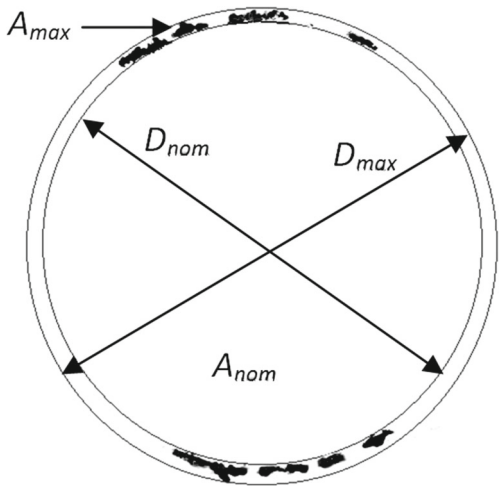

Fig. 6 Scheme of delamination in drilling composite laminate

$$F_d = \frac{D_{max}}{D_{nom}} \tag{14}$$

$$F_a = \frac{A_{max}}{A_{nom}} \tag{15}$$

Whereas A_{max} is the area related to the maximum diameter of the delamination zone D_{max}, A_{nom} is the area of nominal hole D_{nom}.

To process delaminations possessing an irregular pattern when machining CFRP, the adjusted delamination factor F_{da} can be used, and described as follows [31]:

$$F_{da} = F_d + \frac{A_d}{A_{max} - A_{nom}}(F_d^2 - F_d) \tag{16}$$

Thus.

$$\text{If} \begin{cases} A_d \to (A_{max} - A_{nom}) \Longrightarrow F_{da} \to F_d^2 \\ A_d \to 0 \Longrightarrow F_{da} \to F_d \end{cases}$$

Whereas A_d is the delaminated area in the region around the hole.

The first part of Eq. 16 represents the delamination factor or the size of the crack contribution, and the second part represents the damage area contribution.

Tsao et al. [32] concluded that whether the delamination area is minimum or maximum, F_{da} is not equivalent to F_d, also F_{da} is null for minimum and maximum delamination area. Hence, F_{da} is similarly reasonable for regular delamination area. Therefore, a different two-dimensional criterion the equivalent delamination factor (F_{ed}) was proposed to assess the delamination. It is calculated as follows:

$$F_{ed} = \frac{D_e}{D_{nom}} \tag{17}$$

$$D_e = \left[\frac{4(A_d + A_{nom})}{\pi}\right]^{0.5} \tag{18}$$

Whereas D_e is the equivalent delamination diameter.

5 Proposed delamination factor

In this study, the back-up plate has been eliminated when drilling the unidirectional CFRP experimentally and in the FEM simulation.

According to Capello [33], the dynamics of the workpiece acts as an inflected beam, and the force is applied in which the whole drill point acts as a punch on the laminate when using high feed rates makes the delamination mechanism when drilling the workpiece without using the

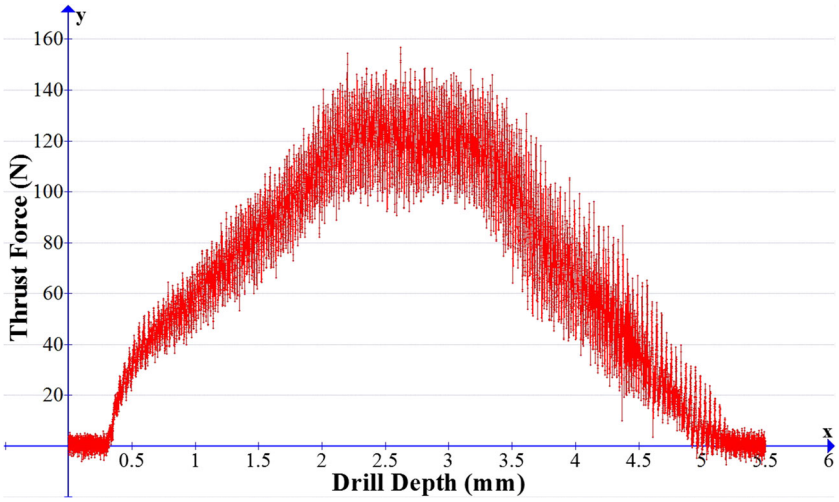

Fig. 7 Thrust force curve measurement

back-up plate more complicated than drilling when using a back-up plate, especially when conventional drilling is still considered the major drilling process used, therefore obtaining the delamination damage becomes more complicated and calculating the delamination factor at the hole entry is a challenge.

The study done by Tsao et al. shows F_{da} and F_{ed} had better recognition results regarding delamination damage when compared to F_d; moreover, the trend of F_d is almost identical to F_{da} and F_{ed}. The experimental results indicated that F_{ed} obtained through digital image processing is considered suitable for characterizing delamination. However, F_{da} is null for the minimum and maximum delamination area and also F_{da} had clearly larger values than F_{ed}.

In this study, firstly, we have implemented F_{ed} instead of F_d and therefore it has a better discrimination of delamination damage results, and secondly to overcome the null critical cases of minimum or maximum delamination area, a new delamination factor called the equivalent adjusted delamination factor F_{eda} is presented below in order to obtain better delamination factors and make it suitable for hole entry delamination.

$$F_{eda} = F_{ed} + \frac{A_{max} - A_{nom} - A_d}{A_{max}}(F_{ed}^2 - F_{ed}) \tag{19}$$

Whereas

$$\beta = \frac{A_{max} - A_{nom} - A_d}{A_{max}} \tag{20}$$

Equation 19 is a combination of the adjusted delamination factor F_{da} representation (size of the crack contribution and the damage area contribution) and the equivalent delamination factor F_{ed} representation (equivalent delamination diameter).

(β) is the delamination free area ratio indicator, i.e., assuming A_{max} and A_{nom} are constant throughout the drilling process, hence whenever A_d increases then β decreases until β becomes zero which indicates that the

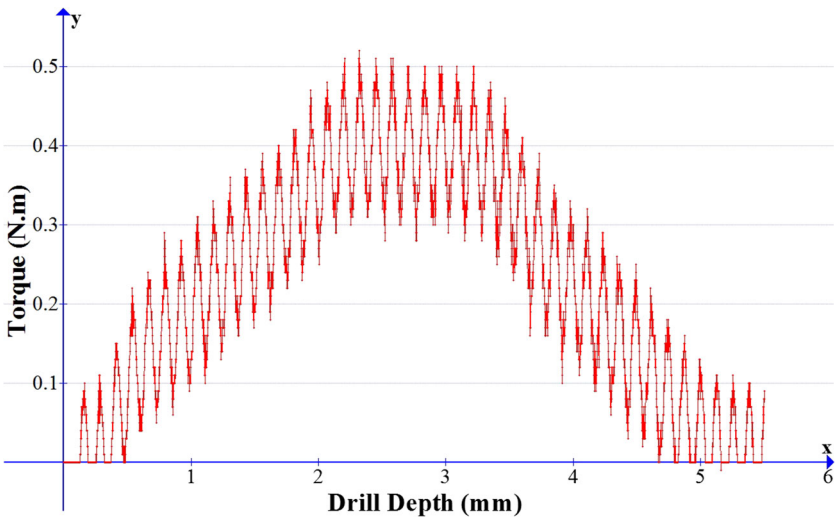

Fig. 8 Torque curve measurement

whole area is delaminated. Also if the delamination area A_d equals zero or maximum, then the second part of Eq. 19 results to zero leading to F_{eda} equaling F_{ed}.

6 Results and discussion

6.1 FE model validation

Thrust force and torque measured in the drilling experiments are calculated and were compared with the results obtained from the new FEA model. Figures 7 and 8 show an example of the force and torque curve measurement in a drilling process. The noises or the oscillations of the signal in Figs. 7 and 8 were caused by the extremely high sampling frequency of the DAQ which was much higher than the rotating frequency of the spindle; in this study, the signals have been processed to utilize the mean values for force and torque.

As mentioned in several studies in literature before [34, 35], the drilling mechanism of CFRP consists of three stages: first stage is the entrance region when the drill starts entering the workpiece; second stage shows a steady state when the drill fully engages with the workpiece, and in this stage the force and torque reach their peak values; the third stage starts with a drop in value until the drill exits the workpiece. Since the thickness for the CFRP plate used in the cutting experiment is only 4 mm, which is very thin in comparison with the diameter of the tool and the value of the feed rate, therefore, the steady drilling process is very short.

Table 6 shows drilling force and torque of experiment and FEA simulation when spindle speed is 5000 rpm and feed rate 500 mm/min for both drills. It can be seen that for PCD drill, the thrust force measured in the experiment was 123.28 N, whereas the FE result showed 118 N; the experiment torque was 0.39 N m and FE torque result was 0.36 N m; the deviation in results ranges approximately between 4 and 8%.

For double-point angle drill, the thrust force measured in the experiment was 127.96 N, whereas the FE result showed 134.86 N; the experiment torque was 0.62 N m and FE torque result was 0.53 N m; the deviation in results ranges approximately between 5 and 15%.

The deviations for FEA when compared to experimental results have occurred due to modeling affects such as the precise modeling of the drill bits or the constitutive properties, but mainly the accuracy between the experiment and the FE simulation results are concluded close and within acceptable range, which indicates the FE model is accurate.

Feed rate is one of the major parameters that affect drilling of composite materials. As shown in Fig. 9a, b for twist drill thrust force and torque analysis, thrust force and torque went up with the increase of feed rate when spindle speed was constant 10,000 rpm. To be specific, thrust force in the experiment was 56 N at 125 mm/min feed rate, the highest was 140 N at 1250 mm/min feed rate, whereas the minimum of FE simulation was of 52 N at 125 mm/min feed rate, and the highest was 134 N at 1250 mm/min feed rate. While the torque in the experiment was 0.11 N m at 125 mm/min feed rate, the highest was 0.44 N m at 1250 mm/min feed rate, whereas the FE estimated 0.1 N m at 125 mm/min feed rate, the highest was 0.42 N m at 1250 mm/min feed rate.

Figure 9c, d shows the thrust force and torque analysis for double-angle point drill, with the same trend as the twist drill; the thrust force and torque went up with the increase of feed rate when spindle speed was constant (10,000 rpm). Thrust force in the experiment was 54.51 N at 125 mm/min feed rate, the highest was 136.88 N at 1250 mm/min feed rate, whereas the minimum of FE simulation was 51.32 N at 125 mm/min feed rate, the highest was 132.76 N at 1250 mm/min feed rate. While the torque in the experiment was 0.28 N m at 125 mm/min feed rate, the highest was 0.55 N m at 1250 mm/min feed rate, whereas the FE estimated 0.2 N m at 125 mm/min feed rate, the highest was 0.53 N m at 1250 mm/min feed rate.

In order to predict how feed rate and spindle speed affect thrust force and torque in the drilling process, a combination of drill feed rate and spindle speed were chosen from Table 7.

For the twist drill, the overall results (Fig. 10a, b) show that thrust force and torque increase with the increase in drill feed rate and decrease with the increase in spindle speed. It was found that thrust force increased by 158% when the drill feed rate increased from 125 to 1250 mm/min at spindle speed of 10,000 rpm, torque increased by 320%. Also

Table 6 Experimental and FEA force and torque measurements for spindle speed 5000 rpm and feed rate 500 mm/min

Drill type	Experimental	FEA	Percent errors	Experimental	FEA	Percent errors
	Thrust force (N)	Thrust force (N)		Torque (N m)	Torque (N m)	
PCD twist drill	123.28	118	4.28	0.39	0.36	7.69
Diamond-coated Double-point Angle drill	127.96	134.86	5.39	0.62	0.53	14.52

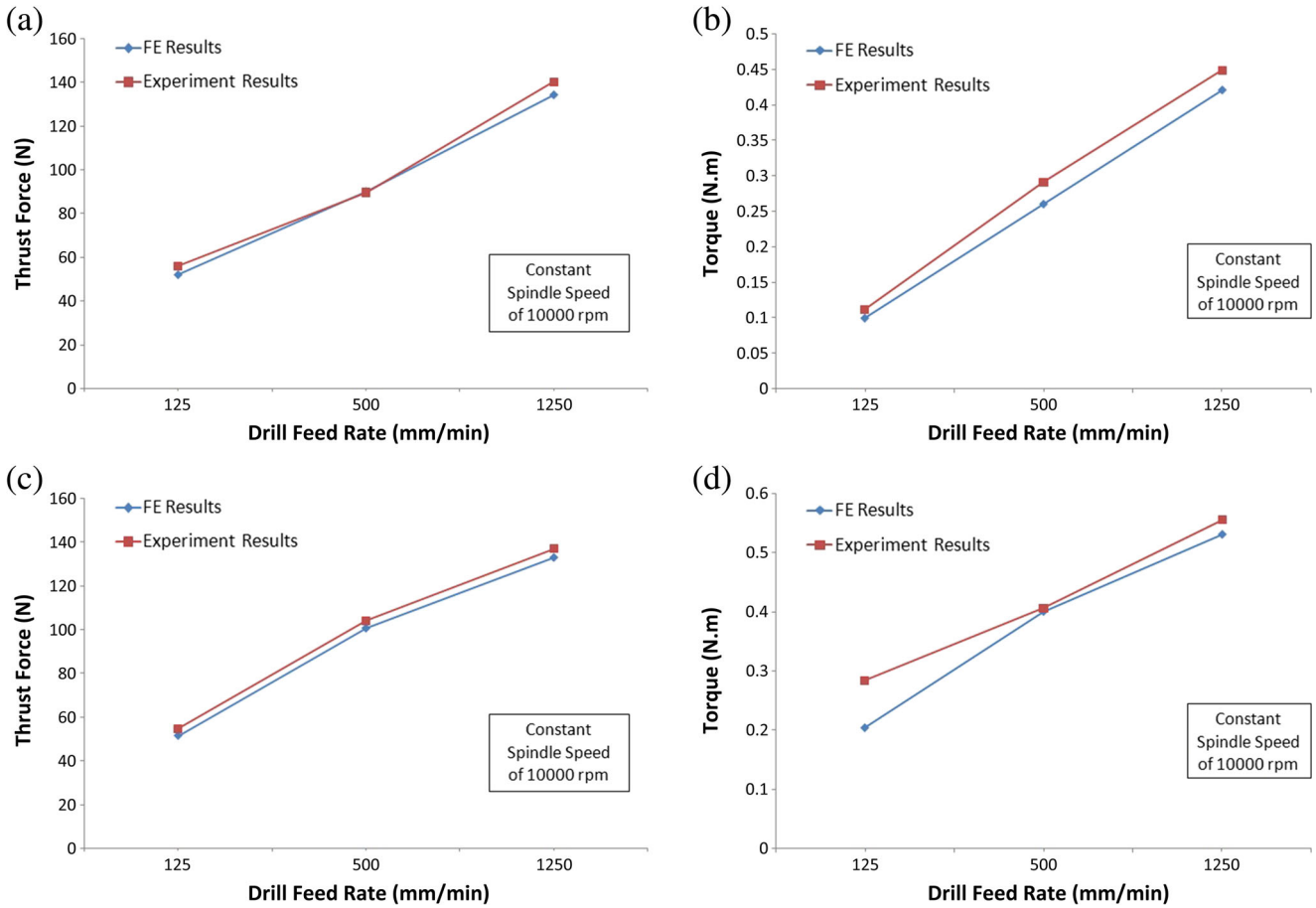

Fig. 9 **a** Twist drill thrust force analysis (Experiment and FE). **b** Twist drill torque analysis (Experiment and FE). **c** Double-point angle drill thrust force analysis (Experiment and FE). **d** Double-point angle drill torque analysis (Experiment and FE)

thrust force decreased by 35% when spindle speed increased from 2500 to 10,000 rpm at 125 mm/min, and the torque decreased by 61%.

For the double-point angle drill, the overall results (Fig. 10c, d) show that thrust force and torque increase with the increase in drill feed rate and decrease with the increase in spindle speed. Thrust force increased by 158% when the drill feed rate increased from 125 to 1250 mm/min at spindle speed of 10,000 rpm, torque increased by 159%. Also, thrust force decreased by 63% when spindle speed increased from 2500 to 10,000 rpm at 125 mm/min, and the torque decreased by 63% as well.

6.2 Delamination factor analysis

To investigate the effect of operating parameters for twist drill and double-point angle drill on the drilling induced damage, the delamination factors obtained in the experimental drilling and finite element analysis were calculated and compared.

Table 7 Cutting parameters used in optimization study

Spindle speed (rpm)	2500, 5000, 10,000, 10,000, 10,000, 7500, 7500
Feed rate (mm/min)	125, 500, 1250, 125, 500, 125, 500

Figure 11 shows results of delamination occurred on the drilled hole entrance peripheral at different cutting parameters. Figures in (a) illustrate the images for experimental drilling with the noises inside the holes filtered, figures in (b) show the acquired delamination areas of figures in (a) after they were processed with ImageJ. Figures in (c) show the FEA simulation results of drilling induced damage. By comparing (b) and (c), it can be seen that the FEA prediction was well estimated and the general delamination trend is very similar to the experiment results.

The experimental delamination factor F_d, the adjusted delamination factor F_{da}, and the equivalent adjusted delamination factor F_{eda} are calculated against the spindle speed and compared in each case for both drills; the results are shown in Fig. 12.

From these results, it can be seen that F_{da} is highest value of the delamination factors, and due to the increase of number of cutting action in the cutting edges at each stage of feed, the trend of delamination factors decreases with the

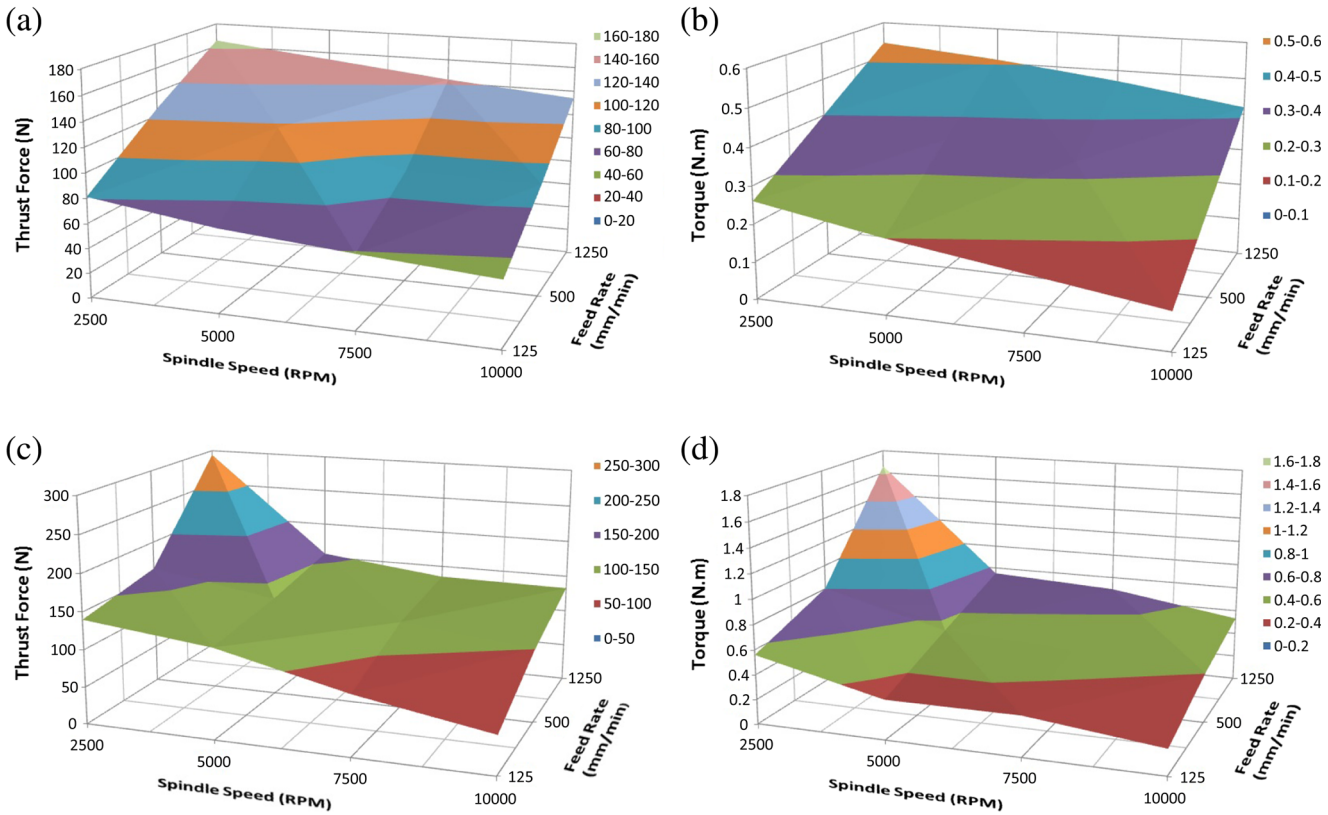

Fig. 10 **a** Effect of twist drill feed rate and spindle speed on thrust force. **b** Effect of twist drill feed rate and spindle speed on torque. **c** Effect of double angle point drill feed rate and spindle speed on thrust force. **d** Effect of double angle point drill feed rate and spindle speed on torque

increase in spindle speed for both drills except for double point drill when it reaches 7500 rpm, as there is a sudden huge increase in delamination factor when it reaches 10,000 rpm, this indicates spindle speed after 7500 rpm is not suitable for double point drill.

For twist drill, it can be noted that when spindle speed increased 300% F_d decreased between 0.63 to 4.1%, F_{da} decreased between 0.8 to 5.0% while F_{eda} decreased between 0.15 to 1.0%.

Regarding the double-point drill, it can be noted that when spindle speed increased 200% F_d decreased between 0.31 to 30.8%, F_{da} decreased between 0.45 to 32.35% while F_{eda} decreased between 0.15 to 4.25%. While if the spindle speed increased 300% F_d increases between 2.79 to 48.53%, F_{da} increased between 4.14 to 53.34% while F_{eda} increased between 2.60 to 6.62%.

The same concept is done for the experimental delamination factors in regards to feed rate for both drills; as shown in Fig. 13 as the increase in feed rate leads to the rise of delamination factors.

For twist drill, the delamination increases drastically when feed rate is over 500 mm/min especially when the feed rate reaches 1250 mm/min.

While for the double point drill, delamination increases drastically when feed rate is over 500 mm/min for spindle speed 2500 and 5000 rpm.

This indicates that feed rate has more effect on delamination than the effect of spindle speed, due to the highly correlation increase of thrust force with the increase of feed rate, which plays a significant role in delamination when drilling composite materials.

To validate simulation results for both drills, F_d, F_{da}, and F_{eda} were calculated and compared for spindle speed of 7500 rpm and feed rates of 125, 500, and 1250 mm/min.

For twist drill, as shown in Table 8 and Fig. 14a, results show that trend of delamination factors is similar to the trend of experimental results, as F_d, F_{da}, and F_{eda} increased 8.8, 22.4, and 12.9% respectively with the increase of feed rate from 125 to 1250 mm/min. The difference in results between experiment and FEA simulation ranges from 4.15 to 4.54% for F_d, 4.82 to 16.69% for F_{da}, and 0.72 to 11.76% for F_{eda} which is a good correlation of output results.

Regarding the double point drill, as shown in Table 9 and Fig. 14b, the same trend for the delamination factors is experienced, as F_d, F_{da}, and F_{eda} increased nearly 1, 2.37, and 1.54% respectively with the increase of feed rate from 125

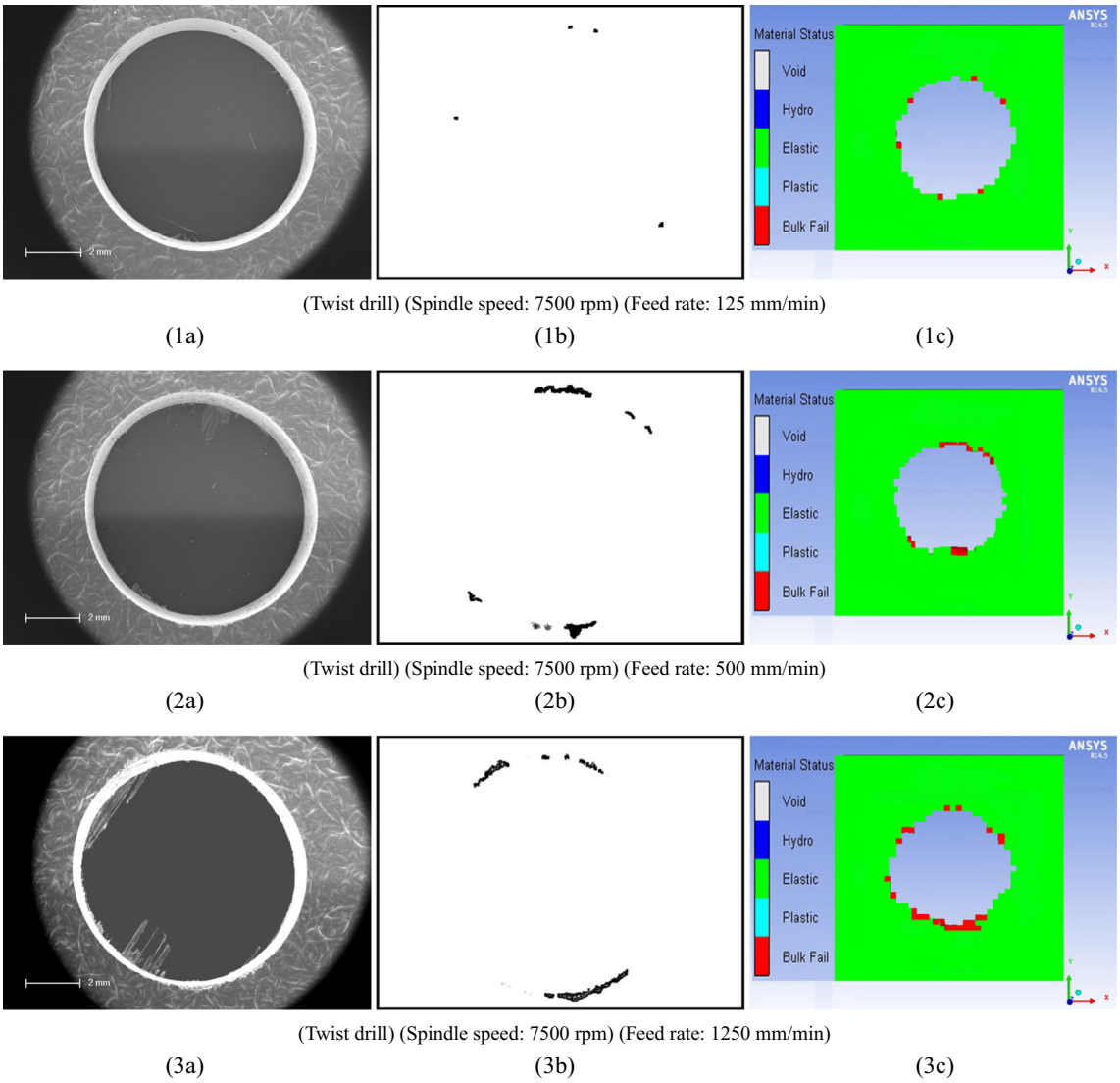

Fig. 11 Delamination analysis for drill entry. **a** Hole images. **b** Experimental delamination areas. **c** Finite element delamination

to 1250 mm/min. The difference in results between experiment and FEA simulation ranges from 4.54 to 4.67% for F_d, 5.6 to 6.98% for F_{da}, and 1.19 to 2.71% for F_{eda}, which again is a good correlation of output results.

It can be seen from the results in Tables 8 and 9 that F_d and F_{da} have close values to each other in both drills whereas the F_{eda} has much lower values due to the effect of F_{ed}, and it shows F_{eda} and F_{da} have better discrimination values than F_d. Also the percentage of errors between the experiment and FEA for F_{eda} is less than F_{da} in the twist drill and it's less than F_d and F_{da} in the double point drill. Table 10 shows an example of the effect of delamination parameters on delamination factors highlighting the delamination free and maximal delamination area effects on delamination factors, it can be seen that F_{da} is null for these two cases whereas F_{eda} is equal to F_d and F_{ed}. This is convincing evidence that the new delamination factor F_{eda} has overcome the null cases and can be used instead of F_{da} for delaminations possessing an irregular pattern.

6.3 Critical thrust force analysis

It is necessary to establish the relationship between thrust force and delamination factor to obtain the critical thrust force at the onset of delamination during the drilling process, hence delamination free holes can be obtained when critical thrust force is predicted if the applied thrust force does not exceed the critical thrust force.

Figure 15 shows the effect of thrust force on the equivalent adjusted delamination factor F_{eda} using the twist and

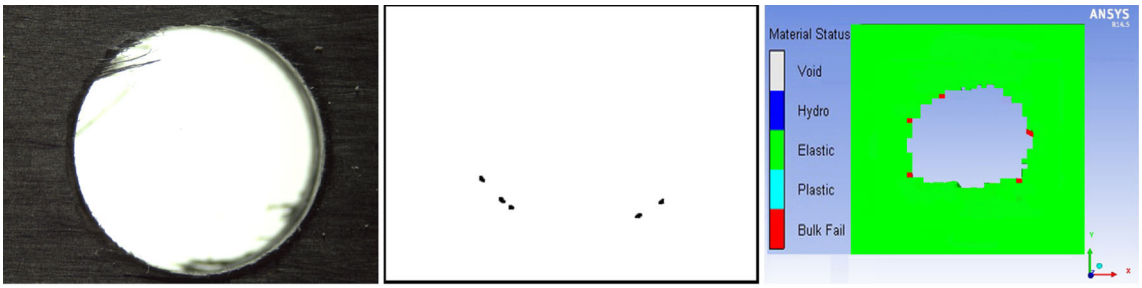

(Double point drill) (Spindle speed: 7500 rpm) (Feed rate: 125 mm/min)

(4a) (4b) (4c)

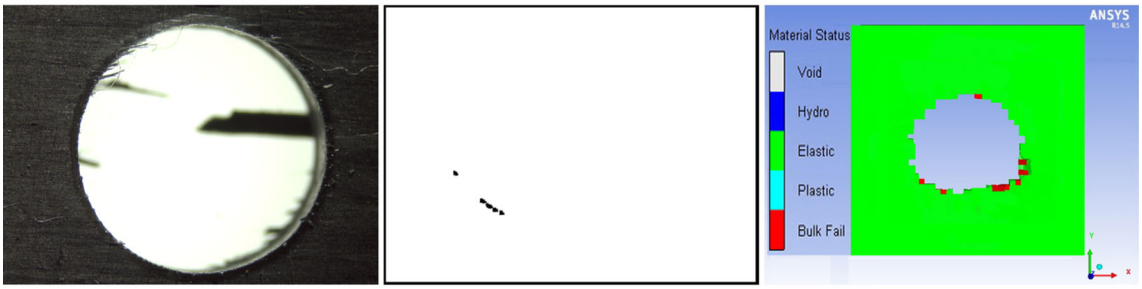

(Double point drill) (Spindle speed: 7500 rpm) (Feed rate: 500 mm/min)

(5a) (5b) (5c)

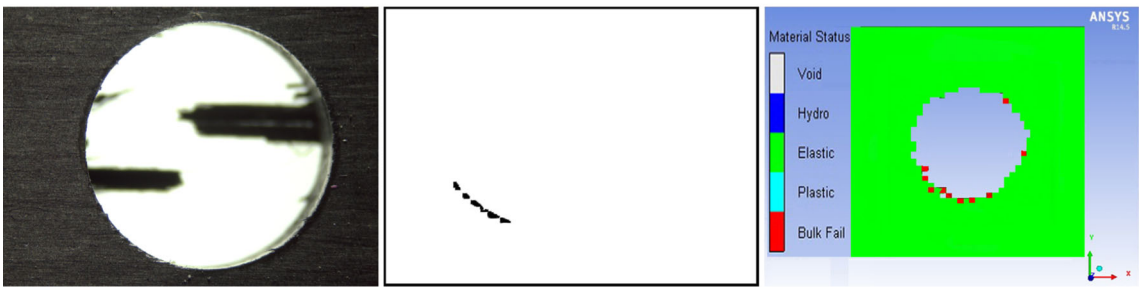

(Double point drill) (Spindle speed: 7500 rpm) (Feed rate: 1250 mm/min)

(6a) (6b) (6c)

Fig. 11 (continued)

double point angle drill. It can be seen that the delamination factor increases with the increase of thrust force, and by using the polynomial function to fit the graphs for each drill bit, we can calculate the critical thrust forces from the below shown equations:

$$F_{tt} = 0.98243746 + 0.00033289 * F_{tt1} \quad (21)$$

$$F_{dd} = 0.62114214 + 0.00634414 * F_{tt2} - 3.3625575 * 10^{-5} F_{tt2}^2 \quad (22)$$

Whereas F_{tt} is the critical thrust force for twist drill; F_{dd} is the critical thrust force for double point angle drill; F_{tt1} is the thrust force for twist drill and F_{tt2} is the thrust force for double point angle drill.

When defining the $F_{tt} = 1$ and $F_{dd} = 1$, then the critical thrust forces for twist drill and double point angle drill will be 59.82 N, 123.34 N respectively; this indicates that the double point drill has a higher safety free-delamination factor approximately 2.1 times the twist drill despite the double-point drill generates higher thrust force than twist drill in most occasions.

Also, by calculating the ratio of thrust force and critical force as shown in equation below, we can define the effect of thrust force on delamination factor.

$$\eta = (F_{tt} - F_{critical})/F_{critical} \quad (23)$$

By applying as an example the critical force and thrust forces values for spindle speed of 5000 rpm and feed rates of 125 mm/min, the calculated ratios of twist drill and double point drill are 17.44 and 0.51% respectively; this leads to the double point drill generates smaller ratios and therefore results in lower delamination factors.

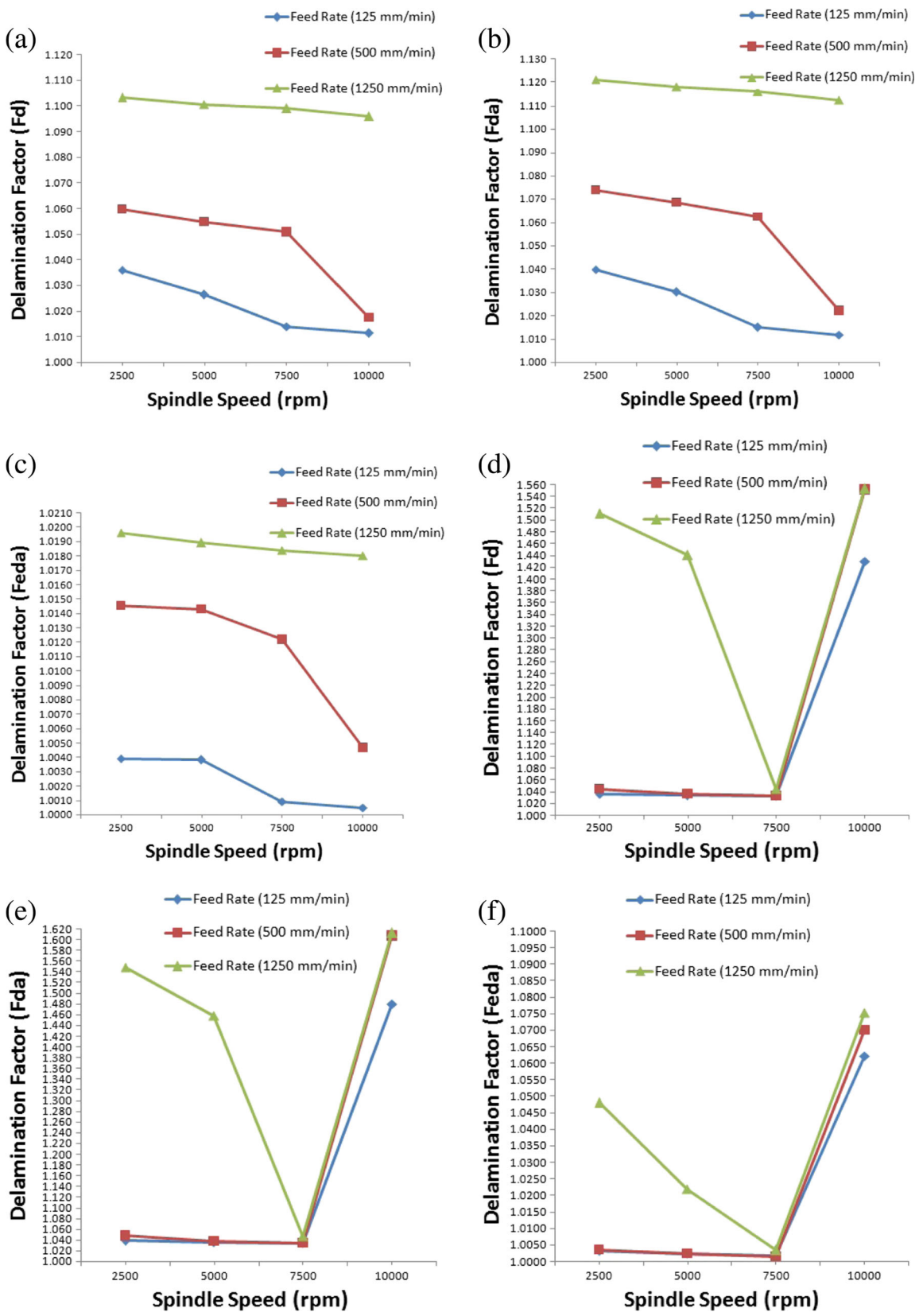

Fig. 12 Effect of spindle speed on experimental delamination factors. **a** Twist drill conventional delamination factor F_d. **b** Twist drill adjusted delamination factor F_{da}. **c** Twist drill equivalent adjusted delamination factor F_{eda}. **d** Double-point drill conventional delamination factor F_d. **e** Double-point drill adjusted delamination factor F_{da}. **f** Double-point drill equivalent adjusted delamination factor F_{eda}

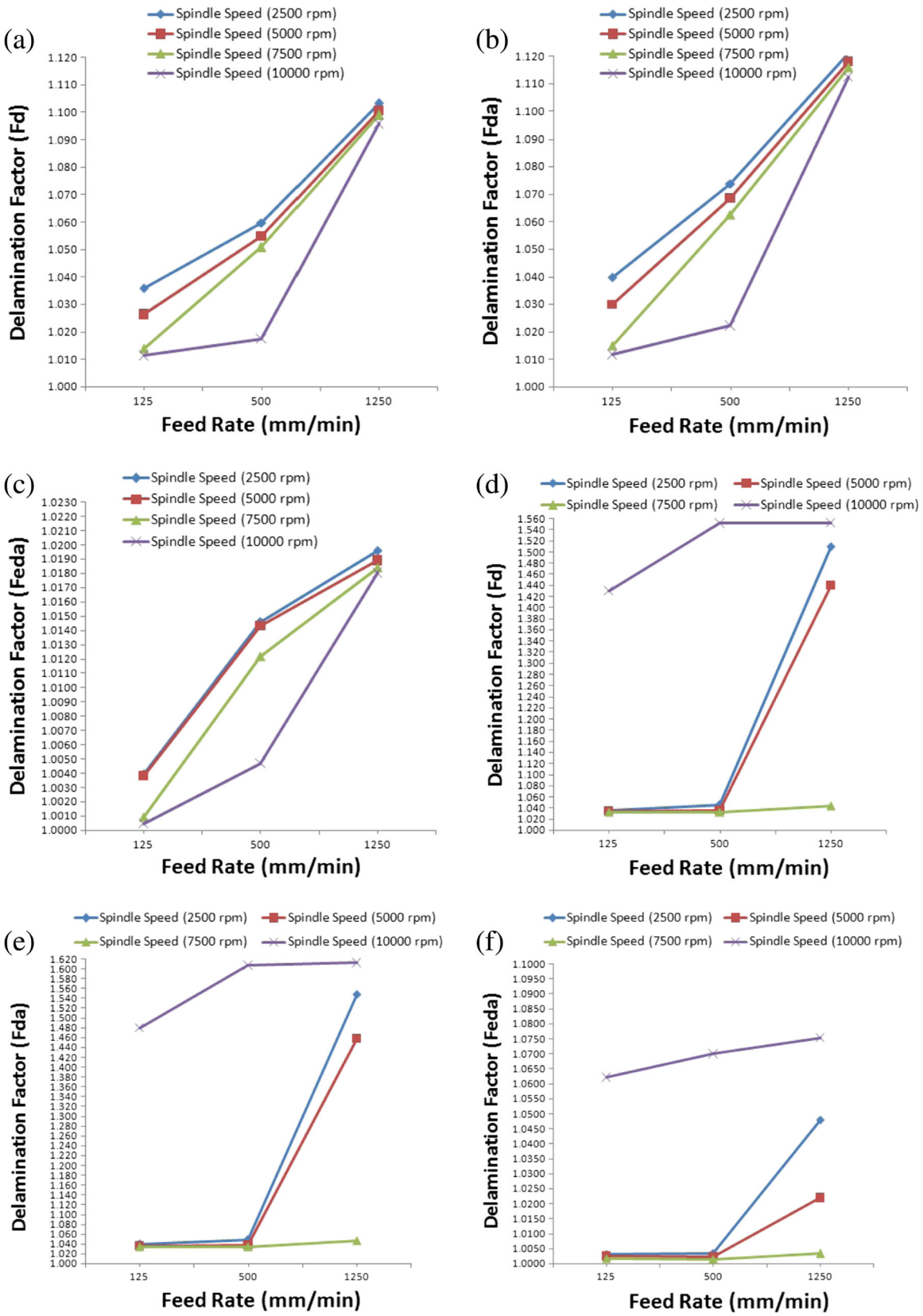

Fig. 13 Effect of feed rate on experimental delamination factors. **a** Twist drill conventional delamination factor F_d. **b** Twist drill adjusted delamination factor F_{da}. **c** Twist drill equivalent adjusted delamination factor F_{eda}. **d** Double point drill conventional delamination factor F_d. **e** Double-point drill adjusted delamination factor F_{da}. **f** Double-point drill equivalent adjusted delamination factor F_{eda}

Table 8 Twist drill delamination factors for experimental and FEA at drill entry

Cutting parameters		Experimental			FEA			Percent errors		
Spindle speed (rpm)	Feed rate (mm/min)	F_d	F_{da}	F_{eda}	F_d	F_{da}	F_{eda}	F_d	F_{da}	F_{eda}
7500	125	1.014	1.015	1.001	1.056	1.064	1.008	4.150	4.820	0.726
7500	500	1.051	1.062	1.012	1.098	1.205	1.097	4.540	13.374	8.379
7500	1250	1.099	1.116	1.018	1.149	1.302	1.138	4.540	16.695	11.764

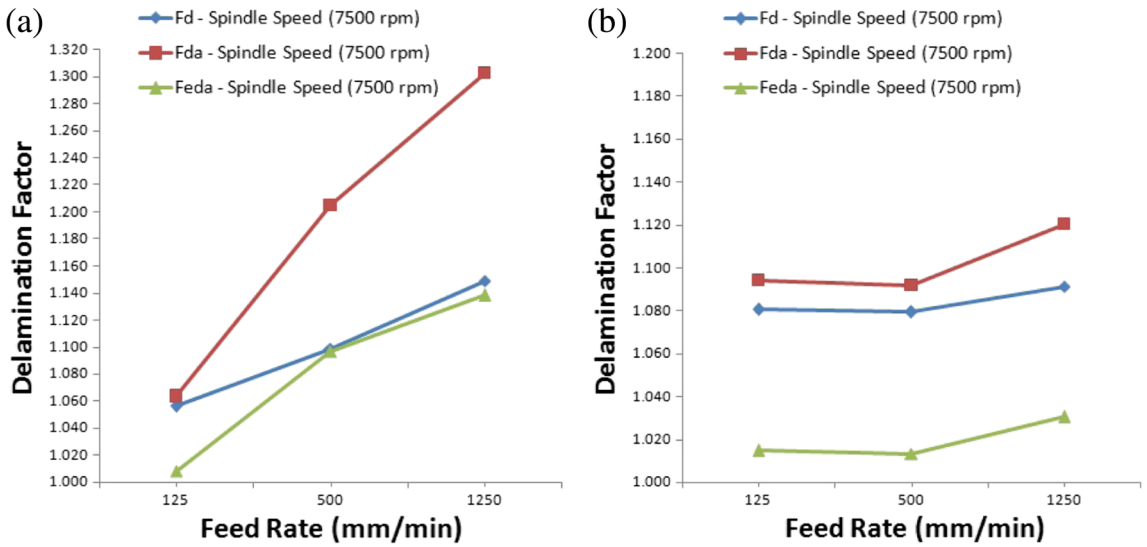

Fig. 14 **a** Effect of feed rate on FEA delamination factors using twist drill. **b** Effect of feed rate on FEA delamination factors using double point drill

Table 9 Double-point drill delamination factors for experimental and FEA at drill entry

Cutting parameters		Experimental			FEA			Percent errors		
Spindle speed (rpm)	Feed rate (mm/min)	F_d	F_{da}	F_{eda}	F_d	F_{da}	F_{eda}	F_d	F_{da}	F_{eda}
7500	125	1.032	1.034	1.002	1.081	1.094	1.015	4.675	5.850	1.315
7500	500	1.033	1.034	1.001	1.079	1.092	1.013	4.540	5.607	1.196
7500	1250	1.044	1.047	1.003	1.091	1.120	1.031	4.540	6.986	2.712

Table 10 Example of the effect of delamination parameters on delamination factors

Test	D_{nom}	D_{max}	A_{nom}	A_{max}	A_d	F_d	F_{da}	F_{ed}	F_{eda}
1	8.000	8.000	50.265	50.265	0.000	1.000	1.000	1.000	1.000
2	8.000	8.112	50.265	51.683	0.091	1.014	1.015	1.001	1.001
3	8.000	8.406	50.265	55.497	1.147	1.051	1.062	1.011	1.012
4	8.000	8.792	50.265	60.711	1.623	1.099	1.116	1.016	1.018
5	8.000	9.000	50.265	63.617	13.352	1.125	1.266	1.125	1.125

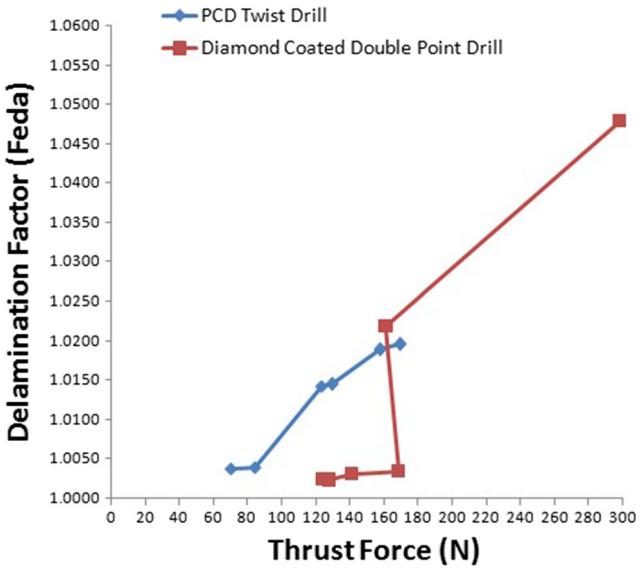

Fig. 15 Effect of thrust force on (F_{eda}) using twist drill and double point drill

7 Conclusion

A great deal of interest has been received lately for progressive damage modeling of polymer matrix composites as predictive capabilities for the complex nonlinear behavior of these materials are sought. Analyzing delamination and evaluating its damage on the CFRP workpiece is very important in determining the structural integrity of the machined part.

In this paper, a new FEA model and new F_{eda} is developed for drilling UDCFRP to study delamination at drilled hole entrance without using a back-up plate. The study is based on utilizing twist drill and double point drill, and by using FEA, results can be evaluated to optimize delamination and parameters can be predicted so further machining and delamination can be prevented.

In this study, the adjusted delamination factor F_{da} was refined to create an equivalent adjusted delamination factor F_{eda} based on F_{ed} and delamination free area ratio, and was able to discriminate the damage values and to overcome the null minimal and maximal delamination values. The trend of variation for F_{eda} is similar to F_d and F_{da}, but F_{eda} had lower percentage error values obtained between the experiment and FEA; all this indicates that the mathematical approach proposed is suitable for characterizing delamination when drilling composites.

Both drills resulted a higher F_{da} than F_d and F_{eda}, as the trend of delamination factors decrease with the increase in spindle speed except for double point drill when it reaches over 7500 rpm; this indicates spindle speed after 7500 rpm is not suitable for double point drill in drilling the CFRP.

Through FEA simulation and experimental analysis, it was found that the thrust force and torque increased with the increase in feed rate and decreased with the increase in spindle speed. Both drills showed a much higher percentage of increase of thrust force and torque when feed rate is increased than the percentage of decrease when spindle speed is increased. Also results showed delamination increases with the increase of feed rate and decreases with the spindle speed, as delamination increased drastically when feed rate is over 500 mm/min; this leads to being feed rate has more effect than spindle speed on hole entry delamination, and it also indicates low feed rates are appropriate for CFRP drilling and the importance of reducing feed rate leads to reducing the axial thrust force to achieve less onset delamination and with better results.

Drill geometry such as point angle and helix angle have high importance in effecting delamination when drilling CFRP; small point angle and low helix angle are preferred for good hole entrance. In this study, both drills have the same helix angle while the double-point angle drill has a primary point angle of 130° which is larger than the twist drill of 120°, which resulted in a higher thrust in most occasions and was evident in the double point angle drill. Results showed in the double point angle drill had less delamination than the twist drill, this is mainly due to its critical thrust force as it possess higher values than the critical thrust force for twist drill; this means the double-point angle drill was highly affected by the critical thrust force and made it better suited for composite drilling as it has a higher safety free-delamination factor approximately 2.1 times the twist drill.

Ply-based modeling is an outstanding base material design and for analyzing mechanisms of composite material behavior and its degradation which are difficult to analyze, while using shell elements reduces the computational time of the simulation process, hence provides an option to model the cutting tool as a flexible body to capture and predict the dynamic effect of machining parameters on the CFRP workpiece . Results of simulations were verified against experimental data, good correlation with experiments has been revealed in terms of predicted delamination area and qualitative representation of external damage.

References

1. Sanda A, Arriola I, Garcia Navas V, Bengoetxea I, Gonzalo O (2016) Ultrasonically assisted drilling of carbon fibre reinforced plastics and Ti6Al4V. J Manuf Process 22:169–176. doi:10.1016/j.jmapro.2016.03.003
2. Isbilir O, Ghassemieh E (2013) Numerical investigation of the effects of drill geometry on drilling induced delamination of carbon fiber reinforced composites. Compos Struct 105:126–133. doi:10.1016/j.compstruct.2013.04.026

3. Wang X, Kwon PY, Sturtevant C, Kim D, Lantrip J (2013) Tool wear of coated drills in drilling CFRP. J Manuf Process 15(1):127–135. doi:10.1016/j.jmapro.2012.09.019
4. Madhavan V, Lipczynski G, Lane B, Whitenton E (2015) Fiber orientation angle effects in machining of unidirectional CFRP laminated composites. J Manuf Process 20, Part 2:431–442. doi:10.1016/j.jmapro.2014.06.001
5. Feito N, López-Puente J, Santiuste C, Miguélez MH (2014) Numerical prediction of delamination in CFRP drilling. Compos Struct 108:677–683. doi:10.1016/j.compstruct.2013.10.014
6. Gudimetla P, Kharidi A, Yarlagadda P (2009) Simulation of delaminations in composite laminates. In: Proceedings of the 6th international conference on precision, meso, micro and nano engineering
7. Durão LMP, Tavares JMRS, de Albuquerque VHC, Gonçalves DJS (2013) Damage evaluation of drilled carbon/epoxy laminates based on area assessment methods. Compos Struct 96:576–583. doi:10.1016/j.compstruct.2012.08.003
8. Grilo TJ, Paulo RMF, Silva CRM, Davim JP (2013) Experimental delamination analyses of CFRPs using different drill geometries. Compos Part B Eng 45(1):1344–1350. doi:10.1016/j.compositesb.2012.07.057
9. Tsao CC, Hocheng H, Chen YC (2012) Delamination reduction in drilling composite materials by active backup force. CIRP Ann Manuf Technol 61(1):91–94. doi:10.1016/j.cirp.2012.03.036
10. Shyha IS, Soo SL, Aspinwall DK, Bradley S, Perry R, Harden P, Dawson S (2011) Hole quality assessment following drilling of metallic-composite stacks. Int J Mach Tools Manuf 51(7–8):569–578. doi:10.1016/j.ijmachtools.2011.04.007
11. Gaitonde V, Karnik S, Rubio JC, Correia AE, Abrão A, Davim JP (2011) A study aimed at minimizing delamination during drilling of CFRP composites. J Compos Mater 45(22):2359–2368
12. Tsao CC (2008) Prediction of thrust force of step drill in drilling composite material by Taguchi method and radial basis function network. Int J Adv Manuf Technol 36(1-2):11–18. doi:10.1007/s00170-006-0808-8
13. Bednarcyk BA, Stier B, Simon J-W, Reese S, Pineda EJ (2015) Meso- and micro-scale modeling of damage in plain weave composites. Compos Struct 121:258–270. doi:10.1016/j.compstruct.2014.11.013
14. Phadnis VA, Makhdum F, Roy A, Silberschmidt VV (2013) Drilling in carbon/epoxy composites: experimental investigations and finite element implementation. Compos A: Appl Sci Manuf 47:41–51. doi:10.1016/j.compositesa.2012.11.020
15. Niezgoda T, Derewońko A (2009) Multiscale composite FEM modeling. Procedia Eng 1(1):209–212. doi:10.1016/j.proeng.2009.06.049
16. Cherniaev A, Telichev I (2015) Meso-scale modeling of hypervelocity impact damage in composite laminates. Compos Part B Eng 74:95–103. doi:10.1016/j.compositesb.2015.01.010
17. Stier B, Simon JW, Reese S (2015) Comparing experimental results to a numerical meso-scale approach for woven fiber reinforced plastics. Compos Struct 122:553–560. doi:10.1016/j.compstruct.2014.12.015
18. Han M-G, Chang S-H (2015) Failure analysis of a Type III hydrogen pressure vessel under impact loading induced by free fall. Compos Struct 127:288–297. doi:10.1016/j.compstruct.2015.03.027
19. Stelzmann IU, Hörmann IM (2011) Ply-based composite modeling with the new* ELEMENT_SHELL_COMPOSITE keyword
20. Halim NFHA, Ascroft H, Barnes S (2017) Analysis of tool wear, cutting force, surface roughness and machining temperature during finishing operation of ultrasonic assisted milling (UAM) of carbon fibre reinforced plastic (CFRP). Procedia Eng 184:185–191. doi:10.1016/j.proeng.2017.04.084
21. Ha SJ, Kim KB, Yang JK, Cho MW (2017) Influence of cutting temperature on carbon fiber-reinforced plastic composites in high-speed machining. J Mech Sci Technol 31(4):1861–1867. doi:10.1007/s12206-017-0333-8
22. Mishnaevsky L (2007) Mesoscale level in the mechanics of materials. Wiley, pp 13–36. doi:10.1002/9780470513170.ch2
23. Burns LA, Mouritz AP, Pook D, Feih S (2012) Strength improvement to composite T-joints under bending through bio-inspired design. Compos A: Appl Sci Manuf 43(11):1971–1980. doi:10.1016/j.compositesa.2012.06.017
24. Sato N, Hojo M, Nishikawa M (2015) Intralaminar fatigue crack growth properties of conventional and interlayer toughened CFRP laminate under mode I loading. Compos A: Appl Sci Manuf 68:202–211. doi:10.1016/j.compositesa.2014.09.031
25. Jones RM (1999) Mechanics of composite materials, 2nd edn. Taylor and Francis, Blacksburg
26. Roos R, Kress G, Ermanni P (2007) A post-processing method for interlaminar normal stresses in doubly curved laminates. Compos Struct 81(3):463–470. doi:10.1016/j.compstruct.2006.09.016
27. ANSYS (2013) ANSYS Composite preppost user's guide Release 15.0 edn. Canonsburg
28. Rakesh PK, Sharma V, Singh I, Kumar D (2011) Delamination in fiber reinforced plastics: a finite element approach. Engineering 03(05):549–549
29. Hashin Z (1980) Failure criteria for unidirectional fiber composites. J Appl Mech 47(2):329–334. doi:10.1115/1.3153664
30. Camanho PP, Dávila CG (2002) Mixed-mode decohesion finite elements for the simulation of delamination in composite materials. NASA/TM-2002-211737
31. Davim JP, Rubio JC, Abrao AM (2007) A novel approach based on digital image analysis to evaluate the delamination factor after drilling composite laminates. Compos Sci Technol 67(9):1939–1945. doi:10.1016/j.compscitech.2006.10.009
32. Tsao CC, Kuo KL, Hsu IC (2012) Evaluation of a novel approach to a delamination factor after drilling composite laminates using a core–saw drill. Int J Adv Manuf Technol 59(5):617–622. doi:10.1007/s00170-011-3532-y
33. Capello E (2004) Workpiece damping and its effect on delamination damage in drilling thin composite laminates. J Mater Process Technol 148(2):186–195
34. Yuan S, Zhang C, Amin M, Fan H, Liu M (2015) Development of a cutting force prediction model based on brittle fracture for carbon fiber reinforced polymers for rotary ultrasonic drilling. Int J Adv Manuf Technol 81(5):1223–1231. doi:10.1007/s00170-015-7269-x
35. Shan C, Dang J, Yan J, Zhang X (2017) Three-dimensional numerical simulation for drilling of 2.5d carbon/carbon composites. Int J Adv Manuf Technol. doi:10.1007/s00170-017-0653-y